

ARTICLE

DOI: 10.1038/s41467-018-05358-3

OPEN

Spin inversion in graphene spin valves by gate-tunable magnetic proximity effect at one-dimensional contacts

Jinsong Xu¹, Simranjeet Singh¹, Jyoti Katoch¹ ¹, Guanzhong Wu¹, Tiancong Zhu¹, Igor Žutić² & Roland K. Kawakami¹

Graphene has remarkable opportunities for spintronics due to its high mobility and long spin diffusion length, especially when encapsulated in hexagonal boron nitride (h-BN). Here, we demonstrate gate-tunable spin transport in such encapsulated graphene-based spin valves with one-dimensional (1D) ferromagnetic edge contacts. An electrostatic backgate tunes the Fermi level of graphene to probe different energy levels of the spin-polarized density of states (DOS) of the 1D ferromagnetic contact, which interact through a magnetic proximity effect (MPE) that induces ferromagnetism in graphene. In contrast to conventional spin valves, where switching between high- and low-resistance configuration requires magnetization reversal by an applied magnetic field or a high-density spin-polarized current, we provide an alternative path with the gate-controlled spin inversion in graphene.

¹Department of Physics, The Ohio State University, Columbus, OH 43210, USA. ²Department of Physics, University at Buffalo, State University of New York, Buffalo, New York 14260, USA. Correspondence and requests for materials should be addressed to R.K.K. (email: kawakami.15@osu.edu)

Spintronics aims for information storage and logic operations by utilizing the electron's spin degree of freedom in addition to its charge. Beyond the three basic processes of spin injection, spin transport, and spin detection, it is crucial to explore new methods of spin manipulation^{1–9} in order to develop novel architectures for spin-based logic. Graphene has become established as an excellent material for spin transport^{10–17}, and there recently have been important advances in the control and modulation of spin transport in graphene spin valves. In graphene with transition metal dichalcogenide (TMD) overlayers, the full modulation of spin currents was demonstrated using electrostatic gates to tune spin absorption into the TMD^{6,8}. In graphene constrictions, the spin transport signal was controlled by gate-tunable quantum interference at low temperatures (<~5 K)³. In graphene spin valves with h-BN tunnel barriers, inversion of spin signal has been observed as a function of bias current¹⁷ and h-BN thickness¹⁸, but gate-dependent inversion of the spin signal was not observed. Alternatively, the MPE in graphene from a ferromagnetic insulator (FI) has been used to fully modulate spin currents by controlling the FI magnetization direction^{7,9}. Beyond these experimental advances, Lazić et al. proposed a different type of MPE from simple ferromagnetic metals that can be used to invert the polarization of spin current as a function of electrostatic gate, but the gate-tunable MPE has yet to be realized^{19,20}.

In this paper, we experimentally demonstrate the gate-tunable MPE in encapsulated graphene spin valves with 1D ferromagnetic edge contacts and observe an inversion of the non-local spin signal as a function of electrostatic backgate voltage. To investigate the origin of the non-local spin signal inversion, we fabricate hybrid spin valves that employ both 1D contacts and traditional top contacts (2D contacts) for spin injector and detector. By comparing the gate-dependent non-local spin signal for injector-detector combinations consisting of 1D–1D contacts vs. 1D–2D contacts, we are able to establish that the inversion of the non-local spin signal originates from an inversion of the effective spin polarization of the 1D contact as a function of gate voltage. This realizes the prediction by Lazić et al.²⁰ that a MPE associated with the spin-dependent DOS of a metallic ferromagnetic electrode could be used to modulate or even invert its effective spin polarization as a function of gate voltage. Unlike 2D contacts where the Fermi level of an adjacent graphene is strongly pinned^{21–23}, the Fermi level of graphene near a 1D contact can be tuned efficiently so that different energy levels of the ferromagnet's spin-polarized DOS can be accessed for gate-tunable MPE. This work provides a new method for manipulating both the magnitude and sign of the spin signal in graphene spin valves, and enables new device architectures for prospective graphene-based spin logic applications.

Results

Device structure and charge transport characterization. Figure 1a shows a scanning electron microscope (SEM) image of one of the measured devices (sample I), and Fig. 1b is a schematic drawing of the device with three types of contacts: 1D transparent contacts, 1D tunneling contacts, or 2D tunneling contacts. The device consists of a h-BN/graphene/h-BN heterostructure on SiO₂(300 nm)/Si substrate (acting as backgate), contacted by nonmagnetic Cr/Au electrodes at two ends and ferromagnetic Co electrodes in between. Details of device fabrication are discussed in the Supplementary Information, Note 1. Figure 1c shows a typical four-probe resistance of graphene as a function of gate voltage, V_{gate} (the channel is 6 μm long and 1 μm wide). This yields a mobility of $\sim 30,000 \text{ cm}^2 \text{ V}^{-1} \text{ s}^{-1}$ for holes and $\sim 20,000 \text{ cm}^2 \text{ V}^{-1} \text{ s}^{-1}$ for electrons. To characterize the contacts, we

perform three-terminal measurement of the differential contact resistance as a function of current bias at 20 K and 300 K (Fig. 1d–f). The 1D transparent contacts exhibit very little variation with either DC bias current or temperature, which is indicative of ohmic conduction (Fig. 1d). For contacts with 0.6 nm SrO barriers, both 1D (Fig. 1e) and 2D (Fig. 1f) contacts show strong bias-dependence of the contact resistance at 20 K, indicating non-ohmic conduction.

Gate-tunable inversion of the spin valve signal. Next, we investigate spin transport with 1D transparent contacts. All measurements are conducted in the non-local geometry (Fig. 2a inset) with lock-in detection and at 20 K. An injection current, I_{INJ} (5 μA rms), is applied between the Co spin injector (E2) and nonmagnetic electrode (E1), and spin transport from E2 to Co spin detector (E3) is measured as a non-local voltage (V_{NL}) measured across E3 and nonmagnetic electrode (E4). The non-local resistance, R_{NL} , is defined as $R_{\text{NL}} = V_{\text{NL}}/I_{\text{INJ}}$. Figure 2a shows R_{NL} as a function of external magnetic field along the Co electrode (B_y) at $V_{\text{gate}} = -40 \text{ V}$. The red (blue) circles are data for increasing (decreasing) B_y . At $\sim 20 \text{ mT}$, an abrupt change in R_{NL} is due to switching of the Co electrode magnetizations from parallel to antiparallel configuration. With further increasing magnetic field, R_{NL} changes back to its original value as the Co electrode magnetizations align parallel. The spin transport is quantified by the change of non-local resistance $\Delta R_{\text{NL}} = R_{\text{NL}}(\text{parallel}) - R_{\text{NL}}(\text{antiparallel})$, which is $\sim 0.2 \Omega$. Interestingly, as gate voltage is tuned to 0 V (Fig. 2b), the curves invert and ΔR_{NL} becomes negative.

To confirm that the non-local signal originates from spin transport, we perform in-plane non-local Hanle spin precession measurements^{24,25} by applying an in-plane external magnetic field B_x perpendicular to Co electrodes. The brown (purple) curves in Fig. 2c, d are the in-plane Hanle curves for the parallel (antiparallel) configuration for $V_{\text{gate}} = -40$ and 0 V, respectively. This verifies the gate-dependent spin inversion with $\Delta R_{\text{NL}} > 0$ for $V_{\text{gate}} = -40 \text{ V}$ and $\Delta R_{\text{NL}} < 0$ for $V_{\text{gate}} = 0 \text{ V}$. The extracted spin lifetimes and spin diffusion lengths are up to $\sim 500 \text{ ps}$ and $\sim 10 \mu\text{m}$ (see Supplementary Note 7). In addition, we further verify that these signals do not originate from local Hall effects associated with magnetic fringe fields or tunneling anisotropic magnetoresistance (see Supplementary Notes 8, 9, and 10). On the other hand, in related work²⁶ the Co electrodes can be specially designed to generate fringe fields up to 0.6 T and produce measurable Hall signals in the non-local geometry.

The detailed gate dependence of the non-local spin signal (Fig. 3a) exhibits a sign reversal at $V_{\text{gate}} \sim -10 \text{ V}$. We note that gate-tunable spin inversion has been observed in most of the 1D edge contacted devices (10 out of 11 samples that exhibited spin signals). In addition, we observe substantial sample-to-sample variations including, in some cases, the polarity of the non-local spin signal changing more than once (see Supplementary Note 2).

Gate-tunable magnetic proximity effect. To understand the origin of the gate-tunable spin inversion, we first rule out quantum interference effects that invert spin signals in small constrictions (few hundred nm) and low temperatures (<5 K)³ because our samples are larger (6 $\mu\text{m} \times 1 \mu\text{m}$) and effects persist up to 75 K (see Supplementary Note 3). Instead, the sign change of ΔR_{NL} is likely due to the spin-dependent DOS of the 1D ferromagnetic contact, which induces ferromagnetism in the graphene via MPE (see Fig. 3d). In metallic ferromagnet/nonmagnet (F/N) bulk-like junctions, e.g., Co/Cu (Fig. 3b, c), the proximity-induced exchange splitting and magnetization, M , decay over a much shorter distance compared to the spin-diffusion length (L_S)

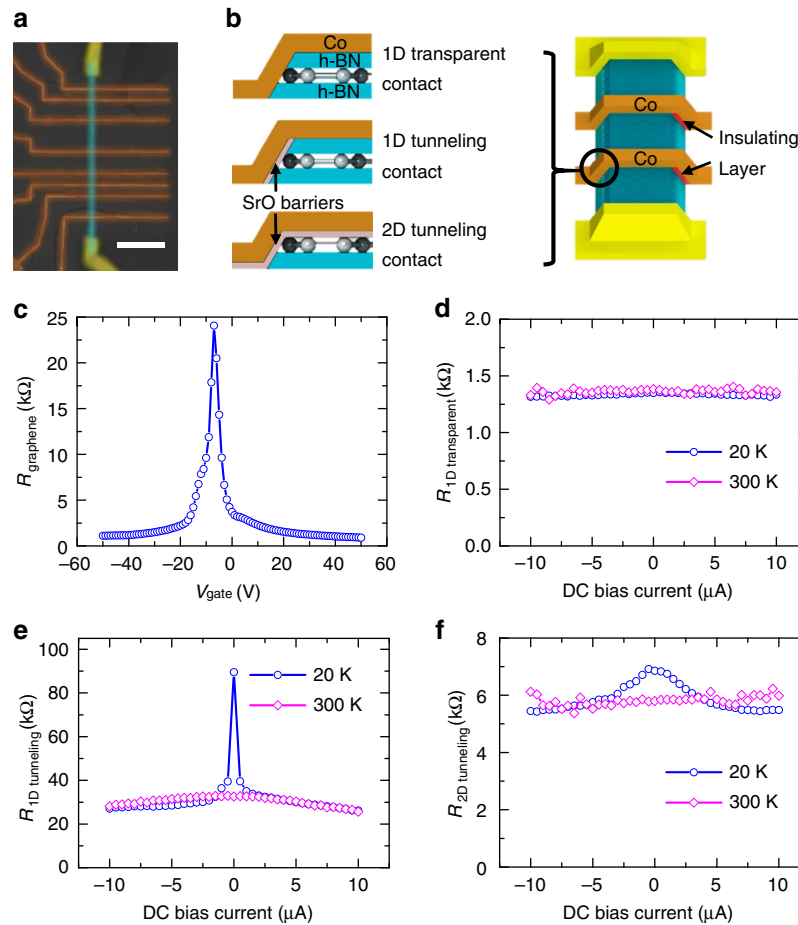


Fig. 1 Electrical characterization of graphene and contact resistances. **a** Scanning electron microscope (SEM) image with false color of one of the measured devices (sample I). The scale bar is 10 μm . **b** Schematic of device and three different types of contacts. Co electrodes (brown color) form two 1D contacts with h-BN/graphene/h-BN heterostructure on two sides. The left side is 1D transparent/tunneling contact, and there is 3 nm thick SrO barrier (red color) isolating Co electrode from h-BN/graphene/h-BN on the right edge. So the current is only injecting from the left edge 1D contact. The yellow color is Cr/Au contact. **c** Gate-dependent graphene resistance (sample I). The channel length is 6 μm and the width is 1 μm . **d–f** Typical bias dependence of the differential contact resistance for 1D transparent contacts, 1D tunneling contacts, and 2D tunneling contacts, respectively. All measurements are done with 0.1 μA AC excitation current

in a nonmagnetic material, which determines the spin injection. Consequently, the description of spin injection usually completely neglects the equilibrium proximity effect in nonmagnetic materials. However, in atomically thin materials such as graphene, the magnetic proximity length exceeds their thickness. The wave functions from the metallic ferromagnet penetrate into graphene, directly polarizing its electronic structure at the Fermi level. Thus, describing spin injection for graphene spin valves with 1D edge contacts should include the MPE²⁰. Instead of occurring at the F/N interface, the spin injection happens at the F* (proximity-modified graphene)/N interface (Fig. 3d). Previously, evidence for such proximity-modified graphene was observed in vertical Co/graphene/NiFe magnetic tunnel junctions, although the two-terminal geometry does not permit backgate tuning²⁷. In addition, X-ray magnetic circular dichroism and angle resolved photoemission experiments directly confirm the magnetic proximity effect for graphene on ferromagnetic metals^{28–30}.

To test whether the inversion of ΔR_{NL} originates from MPE, we need to demonstrate that the effective spin polarization of the 1D contact exhibits a sign reversal. We accomplish this by designing and testing hybrid spin valve devices with both 1D and 2D contacts. Because ΔR_{NL} is roughly proportional to the product of the injector and detector polarization ($\Delta R_{\text{NL}} \sim P_{\text{inj}} P_{\text{det}}$)^{31,32}, one can investigate spin valves with three ferromagnetic electrodes on

the same graphene channel and perform three independent spin transport measurements using the three distinct pairings. Then, one can algebraically extract the effective spin polarization of each contact (see Supplementary Note 4 for details).

Figure 4a, b show the gate dependence of ΔR_{NL} for two hybrid devices (sample II and sample III), each consisting of two 1D transparent contacts (“A” and “B”) and a 2D tunneling contact. The top row is ΔR_{NL} measured using 1D contact A and the 2D contact ($\Delta R_{\text{NL}}^{\text{A*2D}}$), while the second row is ΔR_{NL} measured using 1D contact B and the 2D contact ($\Delta R_{\text{NL}}^{\text{B*2D}}$). Here, the observed inversion of spin signal suggests a polarity reversal of the 1D contact because 2D contacts typically show weak gate dependence (see Supplementary Note 5). The third row is ΔR_{NL} measured using 1D contact A and 1D contact B ($\Delta R_{\text{NL}}^{\text{A*B}}$), while the last row ($\Delta R_{\text{NL}}^{\text{A*2D}} \times \Delta R_{\text{NL}}^{\text{B*2D}}$) is the calculated product of the first two rows. By comparing $\Delta R_{\text{NL}}^{\text{A*B}}$ with $\Delta R_{\text{NL}}^{\text{A*2D}} \times \Delta R_{\text{NL}}^{\text{B*2D}}$, we notice that they are very similar to each other, including both the sign and the trend. Because $\Delta R_{\text{NL}}^{\text{A*B}} \sim P_{\text{A}} P_{\text{B}}$ and $\Delta R_{\text{NL}}^{\text{A*2D}} \times \Delta R_{\text{NL}}^{\text{B*2D}} \sim P_{\text{A}} P_{\text{B}} (P_{\text{2D}})^2$, the similarity of the two curves suggests that P_{2D} has relative little gate dependence, as expected. For quantitative analysis, we utilize the Takahashi–Maekawa model³¹ of non-local spin transport and solve for the effective spin polarizations P_{A} , P_{B} and P_{2D} in terms of the experimental $\Delta R_{\text{NL}}^{\text{A*2D}}$, $\Delta R_{\text{NL}}^{\text{B*2D}}$, and $\Delta R_{\text{NL}}^{\text{A*B}}$ data (see Supplementary Note 4 for

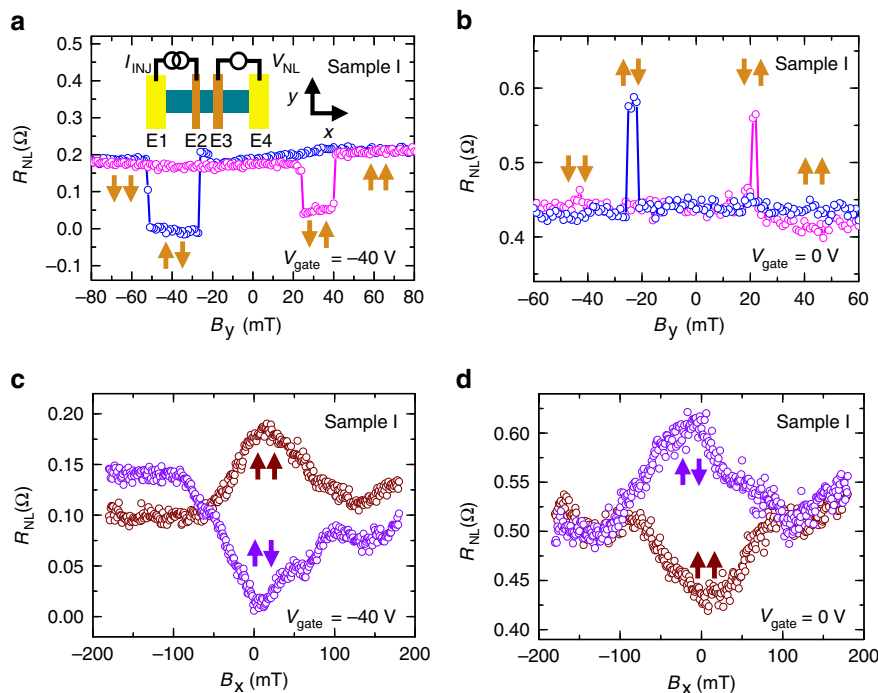


Fig. 2 Spin inversion in graphene spin valves with 1D transparent contacts. **a, b** Non-local spin signal R_{NL} (sample I) for gate voltages of $V_{gate} = -40$ V and $V_{gate} = 0$ V, respectively. The red (blue) curve is for increasing (decreasing) magnetic field. Inset: non-local spin transport geometry. **c, d** Non-local Hanle measurement for gate voltages of $V_{gate} = -40$ V and $V_{gate} = 0$ V, respectively. The brown (purple) curve is for parallel (antiparallel) alignment of the injector and detector magnetizations. The lock-in measurements utilize a $5 \mu\text{A}$ excitation current

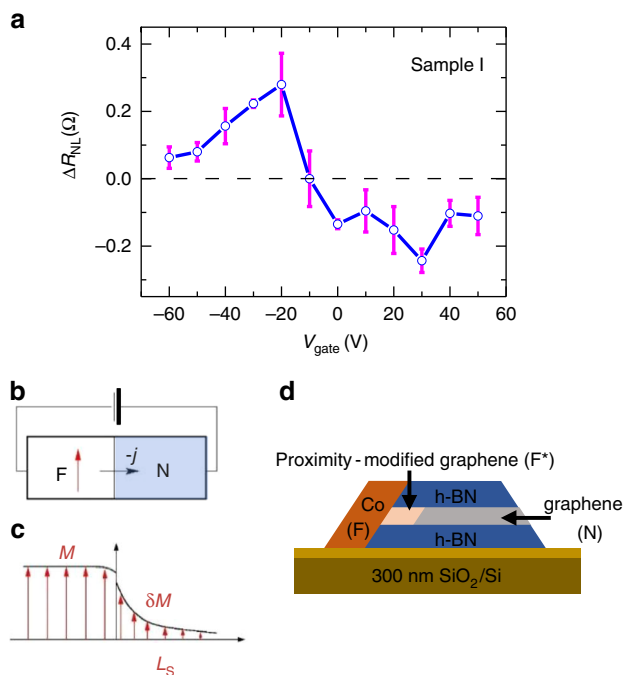


Fig. 3 Gate-tunable magnetic proximity effect at 1D transparent contacts. **a** Gate dependence of the non-local spin signal, ΔR_{NL} (sample I). The error bars correspond to standard error of mean of the non-local MR with increasing and decreasing magnetic field. **b** Schematic of bulk-like metallic ferromagnet/nonmagnet (F/N) junction (e.g., Co/Cu). **c** Spin accumulation in bulk-like F/N junction. **d** Schematic of the magnetic proximity effect for encapsulated graphene with a transparent 1D edge contact to a ferromagnetic electrode

details). The resulting gate-dependent effective spin polarizations are shown in Fig. 4c, d for samples II and III, respectively. Although the two samples have different gate dependences, two important trends are observed in both samples. First, as expected, the effective polarization of the 2D contact, P_{2D} , exhibits relatively little variation with gate voltage. Second, the 1D contacts exhibit polarity inversion as a function of gate voltage. Because the gate-dependent inversion of ΔR_{NL} occurs due to polarity inversion of the 1D contacts, this strongly supports our hypothesis that the spin inversion originates from gate-tunable MPE.

Discussion

Theoretically, this strong gate dependence of the effective spin polarization of the 1D contact comes from the spin-dependent DOS of the 1D interface between graphene and Co as a result of the proximity effect. Lazić et al. reported that the band structure of graphene becomes spin-dependent due to proximity effect to ferromagnetic metals^{19,20}. As a result, one can tune the polarity of spin polarization at the interface through adjusting the Fermi level in graphene by gate voltage. In conventional graphene spin valves with 2D contacts, the Fermi level of graphene underneath the ferromagnetic electrode is strongly pinned and cannot be tuned effectively by gate voltage. This is supported by first-principles calculations^{20,33}, which show that for a 2D contact (e.g., Co/h-BN/graphene), the graphene becomes strongly n-doped: its Dirac cone is shifted ~ 0.5 eV below the Fermi level. A simple electrostatic model²⁰ predicts that the small graphene DOS is required for effective gating. While this could be possible in 2D contacts by shifting the low-DOS region of the Dirac cone close to the Fermi level, it would require a very large gate-induced electric field, more than an order of magnitude larger than ~ 0.2 V nm^{-1} from our experiments (~ 60 V voltage applied on 300 nm $\text{SiO}_2 + \sim 20$ nm h-BN dielectric material). In contrast, our spin valves with 1D contacts form less aggressive contacts with Co which have a much smaller effective n-doping of graphene and

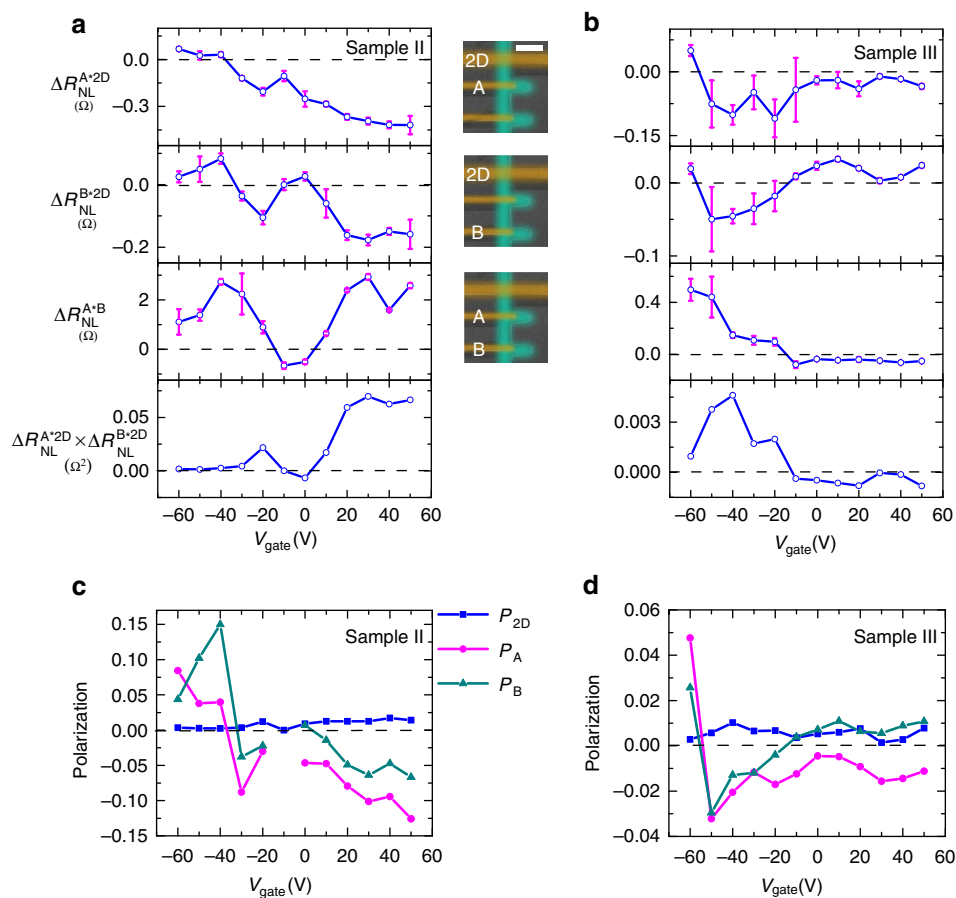


Fig. 4 Spin inversion in hybrid graphene spin valves. **a, b** Gate dependence of ΔR_{NL} for two hybrid devices, sample II and sample III. The spin injector and detector are 1D contact A and 2D contact for the first row, 1D contact B and 2D contact for the second row, 1D contact A and 1D contact B for the third row, respectively, as shown in the central column of SEM images. The scale bar is 2 μm . The last row is the calculated product of the first two rows. **c, d** Effective spin polarization of each contact for sample II and sample III. The error bars correspond to standard error of mean of the non-local MR with increasing and decreasing magnetic field

the shift of the Dirac cone below the Fermi level than what is calculated for 2D contacts^{20,33}. Consequently, in 1D contacts graphene's low-DOS region is attained by a much smaller gate voltage, ensuring that different spin-dependent states are readily accessible by gate tuning. Furthermore, complementary studies of nonlocal spin signal in standard graphene spin valves exhibit spin inversion as a function of bias current¹⁷, and a comparison of different barrier materials (i.e., h-BN, MgO)³⁴ provides evidence for a DOS of Co that reverses spin polarization as a function of energy. Thus, the 1D contacts provide the two necessary ingredients for achieving gate-dependent inversion of the magnetic proximity effect²⁰, namely: (1) having the Dirac point of graphene in the F contact region to be near the Fermi level, where the low DOS in graphene at the Fermi level enables substantial changes in P, and (2) having a ferromagnetic DOS with reversal of spin polarization as a function of energy.

We further examine the MPE by inserting a 0.6 nm SrO tunnel barrier at the 1D contact and again observe gate-tunable spin inversion (see Supplementary Note 6 for details). This demonstrates that the MPE can extend across a tunnel barrier, as predicted theoretically²⁰.

In conclusion, we demonstrate non-local spin transport in h-BN/graphene/h-BN heterostructures with 1D ferromagnetic contacts, and the non-local spin signal can be tuned by gate voltage effectively and even changes polarity. By designing and testing hybrid spin valve devices with both 1D and 2D contacts, we demonstrate this intriguing behavior originates from the gate-

tunable MPE at the 1D contact interface. These results pave the way for future development of graphene spintronics³⁵. Gate-controlled spin polarity may overcome the usual need for an applied magnetic field and a magnetization reversal to implement the graphene-based spin logic³⁶.

Methods

Device fabrication. The general procedure for fabricating h-BN/graphene/h-BN heterostructures is shown in Supplementary Figure 1. First, we mount ~2 mm thick polydimethylsiloxane (PDMS) on a glass slide and cover it with a thin film of polycarbonate (PC). This PC/PDMS stamp is used to pick up top the h-BN flake from an SiO₂/Si substrate. The top h-BN flake is then aligned and brought into contact with graphene on an SiO₂/Si substrate to pick up graphene with this top h-BN flake. Then the whole stack is aligned and brought into contact with the bottom h-BN flake on an SiO₂/Si substrate. After contact, the PC film is cut from the glass slide and the entire PC/h-BN/graphene/h-BN combination remains on SiO₂/Si substrate. The PC film is then dissolved in chloroform. After that, the transferred h-BN/graphene/h-BN heterostructure is cleaned of polymer residue by annealing at 350 °C in ultra-high vacuum (UHV) for 1 h. Then the h-BN/graphene/h-BN graphene heterostructure is patterned by e-beam lithography with PMMA resist and etched by low-power inductively coupled plasma reactive ion etch (ICP-RIE) to get the desired geometry. This process is followed by another annealing step in UHV to remove PMMA residue. Subsequently, we use two steps of e-beam lithography with MMA/PMMA bilayer resist to fabricate electrodes. In the first step, Au electrodes (70 nm) are deposited on the h-BN/graphene/h-BN heterostructure using an e-beam source and a 5 nm Cr underlayer for adhesion. In the second step, Co (60 nm) electrodes are directly deposited in an MBE chamber for one-dimensional (1D) transparent contacts. For tunnel barrier contacts, Co electrodes with SrO tunnel barriers are deposited using angle evaporation with polar angle of 0° for the SrO masking layer (3 nm), 10° for the SrO tunnel barrier (0.6 nm), and 6° for the Co electrode (60 nm). As shown in Supplementary Figure 2, there are a total

of four different device geometries: (1) strip shape with 1D contact, (2) Hall bar shape with 1D contact, (3) 2D contact, and (4) 1D combining with 2D contact. For the strip shape device, on the right edge of the heterostructure, a 3 nm SrO barrier is deposited before Co deposition to form insulating layer to block any conduction. For 2D contact and 1D combining with 2D contact device, the top h-BN, before transfer, is etched with several slits which are used for 2D contact deposition. That is, there is no top h-BN in the red color Co electrode region in Supplementary Figure 2(c) and (d).

Electrical measurements. The measurements are performed in a variable temperature cryostat with vector magnets. The system pressure reaches 1.2×10^{-7} mbar at 20 K. The current is applied using a Keithley 6221 current source and the gate voltage is applied using a Keithley 2400 source meter. The voltage signal is detected with a lock-in.

Data availability. The data that support the findings of this study are available from the corresponding authors on reasonable request.

Received: 14 February 2018 Accepted: 11 June 2018

Published online: 20 July 2018

References

- Datta, S. & Das, B. Electronic analog of the electro-optic modulator. *Appl. Phys. Lett.* **56**, 665–667 (1990).
- Koo, H. C. et al. Control of spin precession in a spin-injected field effect transistor. *Science* **325**, 1515–1518 (2009).
- Guimarães, M. H. D., Zomer, P. J., Vera-Marun, I. J. & van Wees, B. J. Spin-dependent quantum interference in nonlocal graphene spin valves. *Nano. Lett.* **14**, 2952–2956 (2014).
- Wang, Z., Tang, C., Sachs, R., Barlas, Y. & Shi, J. Proximity-induced ferromagnetism in graphene revealed by the anomalous Hall effect. *Phys. Rev. Lett.* **114**, 016603 (2015).
- Wei, P. et al. Strong interfacial exchange field in the graphene/EuS heterostructure. *Nat. Mater.* **15**, 711–717 (2016).
- Yan, W. et al. A two-dimensional spin field-effect switch. *Nat. Commun.* **7**, 13372 (2016).
- Leutenantsmeyer, J. C., Kaverzin, A. A., Wojtaszek, M. & van Wees, B. J. Proximity induced room temperature ferromagnetism in graphene probed with spin currents. *2D Mater.* **4**, 014001 (2016).
- Dankert, A. & Dash, S. P. Electrical gate control of spin current in van der Waals heterostructures at room temperature. *Nat. Commun.* **8**, 16093 (2017).
- Singh, S. et al. Strong modulation of spin currents in bilayer graphene by static and fluctuating proximity exchange fields. *Phys. Rev. Lett.* **118**, 187201 (2017).
- Yang, T.-Y. et al. Observation of long spin-relaxation times in bilayer graphene at room temperature. *Phys. Rev. Lett.* **107**, 047206 (2011).
- Wang, L. et al. One-dimensional electrical contact to a two-dimensional material. *Science* **342**, 614–617 (2013).
- Raes, B. et al. Determination of the spin-lifetime anisotropy in graphene using oblique spin precession. *Nat. Commun.* **7**, 11444 (2016).
- Han, W., Kawakami, R. K., Gmitra, M. & Fabian, J. Graphene spintronics. *Nat. Nanotechnol.* **9**, 794–807 (2014).
- Drögel, M. et al. Spin lifetimes exceeding 12 ns in graphene nonlocal spin valve devices. *Nano. Lett.* **16**, 3533–3539 (2016).
- Singh, S. et al. Nanosecond spin relaxation times in single layer graphene spin valves with hexagonal boron nitride tunnel barriers. *Appl. Phys. Lett.* **109**, 122411 (2016).
- Ingla-Aynés, J., Meijerink, R. J. & van Wees, B. J. Eighty-eight percent directional guiding of spin currents with 90 μm relaxation length in bilayer graphene using carrier drift. *Nano. Lett.* **16**, 4825–4830 (2016).
- Gurram, M., Omar, S. & van Wees, B. J. Bias induced up to 100% spin-injection and detection polarizations in ferromagnet/bilayer-hBN/graphene/hBN heterostructures. *Nat. Commun.* **8**, 248 (2017).
- Kamalakar, M. V., Dankert, A., Kelly, P. J. & Dash, S. P. Inversion of spin signal and spin filtering in ferromagnet/hexagonal boron nitride-graphene van der Waals heterostructures. *Sci. Rep.* **6**, 21168 (2016).
- Lazić, P., Sipahi, G. M., Kawakami, R. K. & Žutić, I. Graphene spintronics: spin injection and proximity effects from first principles. *Phys. Rev. B* **90**, 085429 (2014).
- Lazić, P., Belashchenko, K. D. & Žutić, I. Effective gating and tunable magnetic proximity effects in two-dimensional heterostructures. *Phys. Rev. B* **93**, 241401 (2016).
- Huard, B., Stander, N., Sulpizio, J. A. & Goldhaber-Gordon, D. Evidence of the role of contacts on the observed electron-hole asymmetry in graphene. *Phys. Rev. B* **78**, 121402 (2008).
- Giovannetti, G. et al. Doping graphene with metal contacts. *Phys. Rev. Lett.* **101**, 026803 (2008).
- Xia, F., Perebeinos, V., Lin, Y.-m., Wu, Y. & Avouris, P. The origins and limits of metal-graphene junction resistance. *Nat. Nanotechnol.* **6**, 179–184 (2011).
- Johnson, M. & Silsbee, R. H. Interfacial charge-spin coupling: Injection and detection of spin magnetization in metals. *Phys. Rev. Lett.* **55**, 1790 (1985).
- Jedema, F. J., Heersche, H. B., Filip, A. T., Baselmans, J. J. A. & van Wees, B. J. Electrical detection of spin precession in a metallic mesoscopic spin valve. *Nature* **416**, 713–716 (2002).
- Bogdan, K. et al. 1D ferromagnetic edge contacts to 2D graphene/h-BN heterostructures. *2D Mater.* **5**, 014001 (2018).
- Asshoff, P. U. et al. Magnetoresistance of vertical Co-graphene-NiFe junctions controlled by charge transfer and proximity-induced spin splitting in graphene. *2D Mater.* **4**, 031004 (2017).
- Dedkov, Y. S. & Fonin, M. Electronic and magnetic properties of the graphene-ferromagnet interface. *New J. Phys.* **12**, 125004 (2010).
- Usachov, D. et al. Observation of single-spin Dirac fermions at the graphene/ferromagnet interface. *Nano. Lett.* **15**, 2396–2401 (2015).
- Marchenko, D. et al. Highly spin-polarized Dirac fermions at the graphene/Co interface. *Phys. Rev. B* **91**, 235431 (2015).
- Takahashi, S. & Maekawa, S. Spin injection and detection in magnetic nanostructures. *Phys. Rev. B* **67**, 052409 (2003).
- Sosenko, E., Wei, H. & Aji, V. Effect of contacts on spin lifetime measurements in graphene. *Phys. Rev. B* **89**, 245436 (2014).
- Zollner, K., Gmitra, M., Frank, T. & Fabian, J. Theory of proximity-induced exchange coupling in graphene on hBN/(Co, Ni). *Phys. Rev. B* **94**, 155441 (2016).
- Zhu, T. et al. Probing tunneling spin injection into graphene via bias dependence. Preprint at <https://arxiv.org/abs/1806.06526> (2018).
- Žutić, I., Matos-Abiague, A., Scharf, B., Dery, H., Belashchenko, K. Proximitized materials. Preprint at <https://arxiv.org/abs/1805.07942> (2018).
- Wen, H. et al. Experimental demonstration of XOR operation in graphene magnetologic gates at room temperature. *Phys. Rev. Appl.* **5**, 044003 (2016).

Acknowledgements

We thank Wei Han and Kirill Belashchenko for helpful discussions. Funding for this research was provided by the Center for Emergent Materials: an NSF MRSEC under award number DMR-1420451. We also acknowledge partial support from C-SPIN, one of the six SRC STARnet Centers, sponsored by MARCO and DARPA. Igor Žutić is sponsored by US ONR 000141712793 and NSF-ECCS 1508873.

Author contributions

R.K.K. and J.X. conceived the study and J.X. performed the experiments. S.S., J.K., G.W., and T.Z. contributed to the device fabrication and heterostructure stacking infrastructure. I.Z. led the theoretical analysis. All authors contributed to the analysis and interpretation of the results and preparation of the manuscript.

Additional information

Supplementary Information accompanies this paper at <https://doi.org/10.1038/s41467-018-05358-3>.

Competing interests: The authors declare no competing interests.

Reprints and permission information is available online at <http://npg.nature.com/reprintsandpermissions/>

Publisher's note: Springer Nature remains neutral with regard to jurisdictional claims in published maps and institutional affiliations.



Open Access This article is licensed under a Creative Commons Attribution 4.0 International License, which permits use, sharing, adaptation, distribution and reproduction in any medium or format, as long as you give appropriate credit to the original author(s) and the source, provide a link to the Creative Commons license, and indicate if changes were made. The images or other third party material in this article are included in the article's Creative Commons license, unless indicated otherwise in a credit line to the material. If material is not included in the article's Creative Commons license and your intended use is not permitted by statutory regulation or exceeds the permitted use, you will need to obtain permission directly from the copyright holder. To view a copy of this license, visit <http://creativecommons.org/licenses/by/4.0/>.

© The Author(s) 2018